EMITTANCE EVOLUTION OF LOW ENERGY ANTIPROTON BEAMS IN THE PRESENCE OF DECELERATION AND COOLING*

J. R. Hunt[†1], J. Resta-Lopez[1], C. P. Welsch[1], Cockcroft Institute, WA4 4AD, Warrington, UK
C. Carli, B. Dupuy, D. Gamba, CERN, CH-1211, Geneva, Swizerland
[1]also at the University of Liverpool, L69 3BX, UK

Abstract

The commissioning of the Extra Low Energy Antiproton (ELENA) [1] ring was completed before the start of the second long shutdown (LS2) at CERN. First beams to an experiment in a new experimental zone have also already been delivered. ELENA will begin distributing 100 keV cooled antiproton beams to all antimatter experiments in 2021. This contribution presents measurements made using a novel scraping algorithm capable of determining the emittance of non-Gaussian beams in the presence of dispersive effects. The electron cooler is shown to effectively reduce the transverse phase space after blow-up during deceleration. Finally, the application of the scraping algorithm to other machines with a scraper located in a dispersive region is discussed.

INTRODUCTION

In order to effectively commission and operate any modern storage ring or particle accelerator, it is essential to monitor the transverse emittance of the beam at all stages of the machine's cycle.

A scraper is a method to measure the emittances of very low intensity and energy beams and, thus, was chosen for ELENA. Such a system has been sucessfully in use at the Antiproton Decelerator (AD) for many years [2, 3]. The drawback is that the measurement is destructive for the beam.

When an emittance is measured with a scraper, a scraper blade is moved transversally through the beam. The evolution of the beam loss rate (in some cases the beam intensity) and the scraper position are recorded.

The intensity change may be measured by detecting the secondaries generated by beam interaction with the scraper blade, and is the method used in both the AD and ELENA through the detection of secondary pions with scintillating detectors. ELENA is also capable of supplying H^- to the experimental areas and proton beams may be used for example for electron cooling studies. As a result, micro channel plate (MCP) detectors also comprise the scraper hardware in ELENA, in order to detect the secondary electrons generated by these beams. Once the transverse cumulative density function (CDF) of the beam has been determined through these measurements, analysis may be performed to extract the transverse emittance of the beam.

Generally, the emittance may be calculated using the transverse betatron functions, $\beta_{x,y}$, at the scraper blade's position

and a measurement of the beam width taken from the CDF, as in the AD. In ELENA however, there is no region of zero-dispersion, and so the scraper algorithm must take dispersive effects into account. Additionally, the beam may take on non-Gaussian transverse profiles due to electron cooling and so it is not always possible to assume Gaussian transverse beam distributions [4].

Two new scraper analysis algorithms have been developed for use within ELENA. One method is capable of reconstructing the emittance of Gaussian beams in a region of non-zero dispersion, and estimating the longitudinal RMS relative momentum spread, σ_δ, (here simply RMS momentum spread for brevity). The other algorithm, which requires a combination of successive measurements from both sides of the beam (e.g. positive and negative x), is capable of accurately estimating the emittance for a beam of arbitrary distribution shape. The algorithms have both been previously presented and tested with simulations [5]. In this paper, the new algorithms are used on measurements taken with antiprotons during the commissioning of ELENA in 2018.
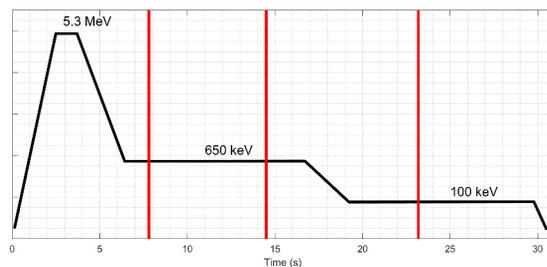

Figure 1: Times measurements were made during the deceleration cycle marked with vertical red lines.

MEASUREMENTS

In total, 16 individual measurements were used for the analysis of the antiproton beam. The measurements were taken at different times along the ELENA deceleration cycle, during energy plateaus, with RF off in order to allow for a coasting beam and Schottky measurements of the RMS momentum spread. An example of a typical ELENA cycle and measurement times may be seen in Fig. 1.

Here we present the measurements taken at $t = 7.8$ s and $t = 14.5$ s along the 650 keV intermediate plateau. Additionally two sets of measurements performed during a second cycle, at the 100 keV ejection plateau are presented. These second measurements were taken at the same time along the plateau, but with cooling off and on to compare effects.

MC6: Beam Instrumentation, Controls, Feedback and Operational Aspects

T03 Beam Diagnostics and Instrumentation

For the RMS emittance in the plane being scraped, $\epsilon_{x,y}$, the two-scan arbitrary beam distribution reconstruction algorithm is as follows:

$$\epsilon_{rms} = \frac{1}{4\beta}\left[\sigma_+^2 + \sigma_-^2 + \frac{(\bar{x}_+ - \bar{x}_-)^2}{2}\right] - \frac{D^2\sigma_\delta^2}{2\beta}, \qquad (1)$$

where D is the dispersion in the scraping plane, σ_δ is an estimation for the RMS longitudinal momentum spread and β is the betatron function of the plane in which the emittance is being measured. Scraping from the two sides gives cumulative density functions (CDFs), $F_\pm$, as seen plotted in Fig. 2. Probability density functions (PDFs), $f_\pm$, are obtained via differentiation of normalised CDFs. The quantities $\sigma_\pm^2$ and $\bar{x}_\pm$ are the RMS and the mean of $f_\pm$, respectively.

To ensure the best possible result, it is essential to clip the data around blade interception with the beam, thus preventing noise (e.g. from injection) contributing to the resultant quantities during integration by incorrectly appearing as high amplitude particle signals. This would occur since detector signal is given as a function of time and later correlated with the scraper's position.

Previously, simulations have shown that for smaller β functions, changes in the closed orbit between scans from opposing directions could contribute towards emittance reconstruction errors. To test typical fluctuations, the mean values of the PDFs, $\bar{x}$, were calculated for two consecutive runs from the same direction, in both planes, x and y. Negligible changes in closed orbit were observed ($\approx$0.04 mm), and the uncertainties derived from such measurements were propagated through the analysis, along with other sources of uncertainty, e.g. $\beta_{x,y}$ calculations.

650 keV Intermediate Plateau

Vertical Measurements Since there is no dispersion in the vertical plane, the beam is easier to diagnose and so these measurements were considered first.

The normalised CDFs obtained from both directions at both times may be seen in Fig. 2. It is possible to observe a small change in the CDFs, reflected in the extracted values for ϵ_y of 1.59 ($\pm$0.02) mm mrad and 1.15 ($\pm$0.02) mm mrad at 7.8 s and 14.5 s, respectively. The values clearly indicate the presence of electron cooling. No significant shift in closed orbit was observed.

A Python [6] script based on Monte Carlo methods, written to generate beam distributions and simulate beam scraping, was used to produce CDFs with corresponding emittances at the same β_y, for Gaussian beams. The resultant CDFs are shown with the measured data in Fig. 2 to allow for a direct comparison. Whilst there is good general agreement in amplitude of measured particles, a better match is observed for measurements at 7.8 s, compared with a tighter core and more populated tails at 14.5 s after some exposure to cooling. This indicates a deviation from Gaussian distributions in the presence of electron cooling, with the beam being more effectively cooled at its core, as expected.
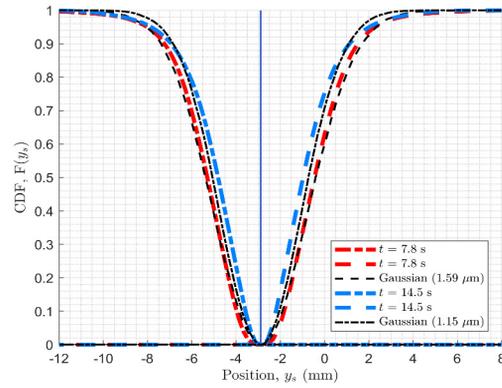

Figure 2: CDFs for vertical measurements during cooling at 650 keV plotted with simulation data ("Gaussian") and (overlaying) closed orbit calculations.

Horizontal Measurements In order to measure the emittance of the beam horizontally, the RMS momentum spread was calculated from Schottky measurements, for input into the reconstruction equation. Figure 3 shows the resultant evolution of the momentum spread during cooling with vertical lines depicting scraper trigger and beam interception times.
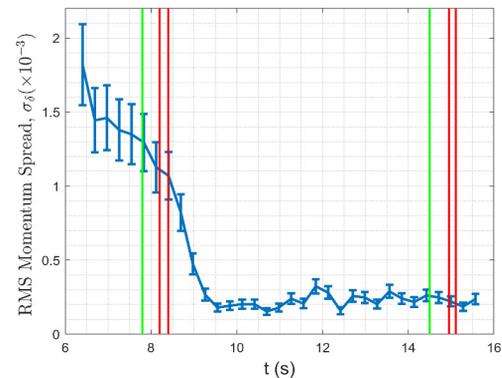

Figure 3: RMS momentum spread during electron cooling at the intermediate plateau. Scraper trigger times are marked with vertical green lines, and resultant beam interception signal was observed at times between two pairs of red lines.

Using extracted σ_δ values of 1.1 ($\pm$0.16) $\times$ 10^{-3} and 0.22 ($\pm$0.03) $\times$ 10^{-3}, the algorithm returned emittances of 3.6 ($\pm$0.27) mm mrad and 0.7 ($\pm$0.05) mm mrad for scraper measurements at 7.8 s and 14.5 s, respectively. This equates to a 81 ($\pm$10)% reduction in emittance over the 6.7 s exposed to electron cooling, which is reflected in a clear difference in the shape of the measured CDFs, Fig. 4. The closed orbit offset of the beam at both times was also calculated by the two-scan algorithm, returning values of -4.05 ($\pm$0.04) mm and -4.22 ($\pm$0.04) mm. This small change in the closed orbit offset during cooling is attributed to a shift in the mean momentum offset, $\bar{\delta}$, of 1.2 ($\pm$0.3) $\times$ 10^{-4}, calculated using $\Delta x_0 = D_x \Delta\bar{\delta}$. With Schottky measurements at a higher harmonic it would be possible to measure $\Delta\bar{\delta}$ more accurately and conversely estimate D_x using this relation and the closed orbit measurements.
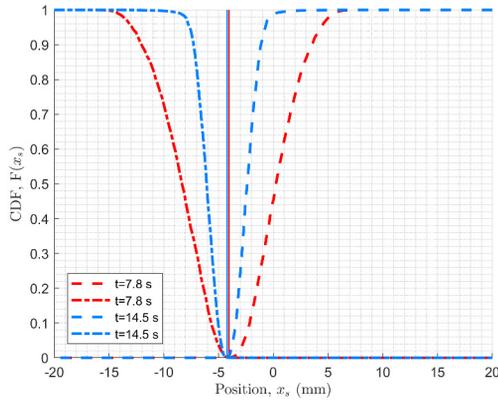
Figure 4: CDFs for horizontal scraper measurements along the 650 keV electron cooling plateau with correspondingly coloured vertical lines at the estimated closed orbits.

100 keV Extraction Plateau

Horizontal and vertical scraper measurements were performed 3.9 s along the extraction plateau with and without electron cooling active. For ϵ_y the emittances were calculated as 2.55 ($\pm$0.03) mm mrad and 0.53 ($\pm$0.01) mm mrad with electron cooling off and on respectively, a reduction of 79 ($\pm$2)%. In the horizontal plane ϵ_x was estimated at 2.5 ($\pm$0.2) mm mrad and 0.55 ($\pm$0.04) mm mrad, a very similar reduction in emittance of 78 ($\pm$10)%. For the horizontal measurements the Guassian fit algorithm was used to estimate the RMS momentum spread, which led to larger uncertainties in the estimates. Analysis of the closed orbit showed a similar shift in the mean momentum offset of $\Delta\bar{\delta} = -1.7\,(\pm0.3)\times10^{-4}$.

Emittance-Momentum Spread Offset Correlation

An emittance-momentum spread offset correlation is expected to arise due to a parabolic distribution of electron velocities centred around $(x, y) = 0$ mm in the electron cooler. The momentum offset of antiprotons with a larger emittance, i.e. of those populating the tails of the beam, is not reduced as effectively as that for particles at the core.

A correlation coefficient derived previously has been shown to accurately give an indication of the magnitude of this effect with simulations. For these measurements the expression has been normalised to the emittance of the beam, to allow for comparison between beams at different stages:

$$\phi_{\epsilon\delta} = \langle(\delta - \bar{\delta})A\rangle\epsilon_x^{-1/2} = \frac{\sigma^2_+ - \sigma^2_-}{4D\sqrt{\beta\epsilon_x}}, \qquad (2)$$

where $\phi_{\epsilon\delta}$ will henceforth be referred to as the correlation coefficient, and δ and A are the momentum offset and amplitude of corresponding particles, respectively.

Table 1 shows the calculated correlation coefficients for both sets of measurements along both energy plateaus. The change in this quantity is positive in both cases, suggesting that electron cooling has brought higher amplitude particles a more positive momentum offset. It should be noted that in both cases the beam already has largely negative correlation

Table 1: Correlation Coefficients with Associated Uncertainties, and Change Between Measurements

	Int. Plat ($\times10^{-5}$)		Ext. Plat ($\times10^{-5}$)	
	$t = 7.8$	$t = 14.5$	No Cooling	Cooling
$\phi_{\epsilon\delta}$	-5.4	1.0	-16	0.3
Error $\phi_{\epsilon\delta}$	2.5	1.1	3.1	0.9
$\Delta\phi_{\epsilon\delta}$	6.4 $\pm$3.6		16.3 $\pm$4	

coefficients, suggesting that the cooler has unintentionally corrected for this characteristic. As a benchmarking exercise, similar analysis for the vertical case showed negligible changes in $\phi_{\epsilon\delta}$, as expected in the absence of dispersion.

CONCLUSIONS AND OUTLOOK

Scraper measurements during cooling have been analysed using a novel scraping algorithm capable of determining the emittance of a non-Gaussian beam in a region of non-zero dispersion. Comparisons of measurements in both transverse planes, along the intermediate and extraction plateaus, show a reduction in emittance in all cases, with particularly significant transverse cooling for both $\epsilon_{x,y}$ at 100 keV. Comparisons of vertical measurements (where dispersion does not convolute the signal) with Gaussian simulations suggests a deviation away from Gaussian distributions after some exposure to electron cooling.

The modest reduction in the vertical emittance along the intermediate plateau could be due to ongoing ELENA commissioning during measurements. Measurements made on separate days for the two plateaus could explain the ratio of emittances between the end of the intermediate plateau and the extraction plateau $2.55/1.15 = 2.22$, being smaller than expected, $(650\,\text{keV}/100\,\text{keV})^{1/2} = 2.55$.

An emittance-momentum offset correlation coefficient has been calculated for the horizontal measurements, and the presence of electron cooling has contributed positively to such an effect. Measurements have shown that after deceleration the correlation tends to be more negative and appears to be unintentionally corrected for after cooling. Further measurements are necessary to fully understand the beam evolution in relation to this effect.

These new algorithms, succesfully used in ELENA, could be applied for other low and medium energy storage rings equipped with scraping hardware in a dispersive region. Since the algorithms do not require additional hardware (other than to scrape from both sides in each plane), they can be easily implemented. In particular, since such techniques have been shown so effective for low energy antiprotons, next generation antimatter facilities, such as FLAIR at FAIR could benefit from their use [7].

ACKNOWLEDGEMENTS

REFERENCES

[1] V. Chohan *et al.*, "Extra Low ENergy Antiproton (ELENA) ring and its Transfer Lines: Design Report," Tech. Report, CERN-2014-002, Apr. 2014.

[2] S. Maury, "The Antiproton Decelerator: AD", Hyperfine Interactions, vol. 109, no. 1/4, pp. 43-52, 1997.

[3] M. E. Angoletta *et al.*, "Beam Measurement Systems for the CERN Antiproton Decelerator (AD)," in 19th IEEE Particle Accelerator Conference, Chicago, IL, USA, Jul. 2001.

[4] J. Resta-Lopez *et al.* "Non-Gaussian beam dynamics in low energy antiproton storage rings," Nucl. Instr. Meth. A, vol. 834, pp. 123-131, Oct. 2016.

[5] J. R. Hunt *et al.*, "Emittance measurements in low energy ion storage rings," Nucl. Instr. Meth. A: , vol. 896, pp. 139-151, Jul. 2018.

[6] "Python" https://www.python.org/

[7] "Facility for Low-Energy Antiproton and Ion Research" http://www.flairatfair.co.uk/